2D IR Spectroscopy using Four-Wave Mixing, Pulse Shaping, and IR Upconversion: A Quantitative Comparison

William Rock[a,‡], **Yun-Liang Li**[a], **Philip Pagano**, and **Christopher M. Cheatum**[*]
Department of Chemistry and Optical Science and Technology Center, University of Iowa, Iowa City, IA 52242

Abstract

Recent technological advances have led to major changes in the apparatuses used to collect 2D IR spectra. Pulse shaping offers several advantages including rapid data collection, inherent phase stability, and phase cycling capabilities. Visible array detection via upconversion allows the use of visible detectors that are cheaper, faster, more sensitive, and less noisy than IR detectors. However, despite these advantages, many researchers are reluctant to implement these technologies. Here we present a quantitative study of the S/N of 2D IR spectra collected with a traditional four-wave mixing (FWM) apparatus, with a pulse shaping apparatus, and with visible detection via upconversion to address the question of whether or not weak chromophores at low concentrations are still accessible with such an apparatus. We find that the enhanced averaging capability of the pulse shaping apparatus enables the detection of small signals that would be challenging to measure even with the traditional FWM apparatus, and we demonstrate this ability on a sample of cyanylated dihydrofolate reductase (DHFR).

Keywords

2D IR; IR Pulse Shaping; Four-Wave Mixing

Introduction

Two-dimensional infrared spectroscopy (2D IR) can reveal kinetic and dynamic information on a myriad of molecular systems.[1] Despite the wealth of information that 2D IR can provide, relatively few research groups utilize this technique because 2D IR spectrometers are expensive and difficult to build and operate. The Zanni group has shown that direct infrared (IR) pulse shaping simplifies 2D IR data collection and analysis,[1–11] and similar approaches have been employed for 2D electronic spectroscopy as well.[12–16] We have developed a detection system that uses a visible CMOS array to measure upconverted IR as an inexpensive alternative to liquid-nitrogen-cooled mercury-cadmium-telluride (MCT) arrays.[17] Together, these technological developments may allow more research groups to use 2D IR spectroscopy in the future.

Despite the advantages that pulse shaping and upconversion detection offer, these methods have not yet been widely adopted in the 2D IR community, in part because many researchers fear that these techniques could adversely impact the limit of detection and signal-to-noise ratio (S/N) enough to make some experiments inaccessible. Although both technologies

[*]Author to whom correspondence should be sent: Christopher M. Cheatum Department of Chemistry, University of Iowa, Iowa City, IA 52242, 319-353-0379, christopher-cheatum@uiowa.edu.
[a]Authors contributed equally to this work
[‡]Present address: Max Planck Institute for Polymer Research, Mainz, Germany

should, in principle, reduce the size of the observed signal and the S/N, no studies have quantified the severity of these effects in practice. Kumar, Tamimi, and Fayer recently reported a comparison of the spectral diffusion measured using a pulse shaper in the rotating frame with that measured using a more conventional 2D IR spectrometer.[18] Over a relatively narrow frequency range of interest and with modest linear absorbance, as is often the case in 2D IR, the lineshapes from these measurements should be the same leading to the same experimental FFCF,[19–21] and their experiments confirmed this expectation. They did not however, address the more significant question of what experiments will be accessible with a pulse shaper. In particular: Will it still be possible to measure the spectral diffusion for weak chromophores in dilute solutions such as for proteins?

The most commonly used experimental apparatus for 2D IR spectroscopy, the socalled four-wave mixing (FWM) apparatus, uses a multiple-beam interferometer to generate three independently controlled beams that focus into the sample in a so-called "boxcar" geometry to produce a vibrational echo response. The vibrational echo is background-free. Thus, the intensities of the input beams are only limited by the amount of available light. After the sample, the vibrational echo overlaps with a local oscillator for heterodyned detection.

A pulse shaper transforms a pump-probe spectrometer into a 2D IR spectrometer. For the same total power, the signal in the pump-probe geometry will necessarily be less than in the boxcar geometry because the pump-probe experiment is a self-heterodyned measurement, which means the probe beam provides both the third electric field and the local oscillator. Independent control of the power of the third electric field and the local oscillator does not exist. Because the probe beam illuminates the detector in the pumpprobe geometry, the dynamic range of the detector places an upper limit on the intensity of the probe pulse and, therefore, the third electric field that gives rise to the signal.

Although the signal in the pump-probe geometry is inherently smaller than that for FWM,[22] a pulse shaper offers several advantages. In the FWM apparatus, mechanical delay lines controlled by computerized stages determine the relative timings of the pulses, most importantly the time delays between pulses one and two and between the signal and local oscillator. The inherent uncertainty in the exact zero of those time delays results in spectra with phasing ambiguity after Fourier transformation into the frequency domain. One must correct this phase error using the projection-slice theorem, which says that the 2D IR spectrum integrated over ω_1 must reproduce the frequency-dispersed pump-probe spectrum. So, by independently measuring a pump-probe spectrum for the same waiting time, we can adjust the phase of the 2D IR spectrum so that the corrected spectrum obeys the projection-slice theorem. Therefore, every 2D spectrum requires the measurement of the appropriate pump-probe spectrum to properly phase the data, effectively setting the detection limit to the weakest measurable pump-probe spectrum. This limitation can be particularly problematic in a conventional FWM apparatus because the total IR intensity is divided evenly among the three excitation pathways, which is not optimal for pump-probe experiments. In the case of the pulse-shaper apparatus, self-heterodyned detection and the near-perfect control over the time delay between the first two pulses eliminate the phase errors. As a result, the spectra obtained using the pulse shaper are correctly phased as measured and can be automatically averaged without correction during data processing.

In addition to the inherent phase stability and accurate timings, the pulse shaper also acquires data very rapidly and maximizes the available signal while minimizing contributions from scattered light. The pulse shaper also controls the phases of the two pump beams it generates. NMR spectroscopists were the first to realize the benefits of phase control, including phase cycling and phase incrementing, which are widely used in modern NMR spectroscopy. Phase cycling allows for isolation of the desired signal from scattered

light and other contributions that come out on top of the probe beam without chopping the pump beam, and phase incrementing shifts the observed carrier frequency to a longer wavelength, which allows a larger fully sampled step size.

Recent efforts have demonstrated improvements to the traditional FWM apparatus that provide many of these benefits of pulse shaping without a pulse shaper. Balanced detection allows for additive signals while subtracting away unwanted pathways and scattered light.[23] Continuous scanning of the translation stages enables rapid data collection with a mechanical stage.[24, 25] Specialized optics such as a wobbling Brewster window can create sub-cycle delays for a quasi-phase cycling technique.[26] Active-phase stabilization of the FWM apparatus can reduce phase drift and improve the accuracy of the time axis of the delay stages,[27, 28] which is effective at reducing phase drift and accurately determining the time delays but adds experimental complexity to the FWM apparatus. Finally, one can correct the phase error of the delay lines by presetting the phase using the interference patterns formed by the pulse pairs (1,2 and 3,LO) in the boxcar geometry at the focal plane of the experiment,[29] but this process is tedious, as it involves scanning a very small pinhole at the focal plane to map out the interference patterns for each pulse pair, and it must be repeated periodically to correct for imperfect phase stability even with a phase-stabilized apparatus.

Although these optimizations of the FWM apparatus realize most of the advantages of using a pulse shaper, they add considerable complexity to the experimental apparatus and do not, in general, result in a complete or trouble-free solution to the phase problems. Ultimately, we do not compare the pulse-shaping apparatus to a fully optimized FWM apparatus with continuous scanning, balanced detection, phase stabilization, and absolute phase correction, which would certainly show superior S/N. Rather, we compare to a more conventional FWM apparatus similar to that used by most researchers in the field with stepped mechanical delays and signal isolated by a chopper in one arm of the interferometer. Our aim is to address how the signal-to-noise and limit of detection of a pulse shaper apparatus compare to those of a more conventional FWM apparatus and whether or not the signals from weak chromophores in dilute solutions will be accessible with a pulse-shaper apparatus as these are the central questions that limit the widespread adoption of this method.

Many practitioners of 2D IR spectroscopy use MCT array detectors to increase the rate of data collection, but IR arrays are extremely costly and lack the sensitivity and pixel density of cheaper visible arrays. Upconversion of the IR electric field in an appropriate nonlinear optical (NLO) crystal is an effective strategy to gain the benefits of visible detection in the IR, a strategy that has been employed for many years.[30–32] The simplest upconversion setups use a narrow-band visible source to upconvert the IR spectrum for visible detection. In this arrangement, the frequencies in the IR spectrum are given by the difference between the measured upconverted spectral frequencies and the frequency of the narrow-band visible light. One alternative to this approach that has been used for 2D IR spectroscopy is chirped-pulse upconversion, which collects vibrational spectra with a visible array using the zero-order reflection from the compressor grating in a Ti:Sapphire amplifier as the upconversion source.[33, 34] This technique cleverly uses a source of visible light that is discarded in most optical setups. The uncompressed 800 nm light, strictly speaking, is a broadband source, but only a small portion of the visible bandwidth temporally overlaps with the fs IR pulse in the NLO crystal because of the large chirp on the pulse. DeCamp and Tokmakoff demonstrated another approach to upconversion in which a grating spectrally disperses the IR beam spatially onto a wide (8 mm) NLO crystal, and a broadband femtosecond 800 nm pulse mixes with the IR in the NLO crystal.[35] The spatial dispersion of the IR before the NLO crystal provides the spectral resolution of the upconverted light, which the bandwidth of the visible source does not limit.

In our group, we have developed an apparatus that uses bandwidth-narrowed 800 nm light to do sum-frequency-generation in a MgO-doped LiNbO$_3$ crystal.[17] Only half of our laser output pumps our OPA. The rest is available for upconverting the IR. A three-optic zero-dispersion stretcher with a variable-width slit at the Fourier plane narrows the bandwidth of the 800 nm beam before mixing with the IR. The unique feature of our setup is the CMOS array detector that we use to measure the spectrum. A 1024-pixel single-line CMOS array (Imaging Solutions Group LW-ELIS-1394A) placed at the focal plane of the spectrometer measures the upconverted probe spectrum on every laser shot. This array has a much higher pixel density than IR arrays and is a very low-cost (<1500 USD) detector compared to MCT or CCD arrays. In addition, the camera collects spectra at a maximum line-rate of 10 kHz, meaning that this same detector could be used with laser systems having a much higher repetition rate than is commonly used today. In principle, visible detection by upconverting the IR light should reduce the S/N of a 2D IR spectrometer by introducing an additional nonlinear optical process that should add noise to the measurement. Nobody, however, has tested the practical impact of visible detection on the S/N of a 2D IR experiment with a weak chromophore, and it is difficult to predict.

This manuscript compares the signal-to-noise ratio measured using a traditional FWM apparatus and a pulse-shaping apparatus while keeping as many experimental variables as possible constant. This manuscript also compares the measured S/N of the pulse-shaping apparatus with single-channel IR detection and with upconversion and CMOS-array detection. Although we do identify some of the potential sources of the differences we observe, we do not attempt to exhaustively study and attribute these differences as we are most interested in identifying the limit of detection of the pulseshaper with upconversion apparatus. We use a dilute solution of methylthiocyanate (MeSCN) in dimethylformamide (DMF) as the probe molecule for the comparison. MeSCN absorbs at 2155 cm^{-1} in DMF and is a relatively weak chromophore (ε 200 M^{-1} cm^{-1}) by 2D IR standards. We choose DMF, a background-free solvent, to eliminate errors in the measurement of the S/N that might occur because of a solvent background. Finally, we also demonstrate the feasibility of experiments on weak chromophores in dilute solutions using the pulse-shaper apparatus by measuring a 2D IR spectrum of the protein dihydrofolate reductase (DHFR) with two cyanylated cysteine labels.

Experimental

We base the two different 2D IR experimental setups used in this work on identical amplified Ti:Sapphire laser systems (Spitfire Pro) that output 800 nm pulses at a 1 kHz repetition rate. The pulses are 90 fs in duration with about 4 mJ of pulse energy. A 5:3 reflective telescope reduces the beam diameter, and then a 50/50 beam splitter divides the beam. Approximately 800 µJ/pulse of the reflected light pumps a home-built two-pass optical parametric amplifier (OPA) based on a β-barium borate (BBO) crystal (θ=27°, type II). The energy difference between the signal and idler beams from the OPA is tunable, and we adjust this difference to the desired mid-IR frequency. Difference frequency generation (DFG) of the signal and idler in a AgGaS2 crystal (θ=50°, type II) produces the desired mid-IR radiation. Both systems produce 6 µJ mid-IR pulses 130 fs in duration, centered at 2155 cm^{-1} with a full-width at half-maximum (FWHM) of 115 cm^{-1}. We carefully kept the power, pulse duration, and focusing conditions of both systems as identical as possible. The optical setups of the 2D IR spectrometers differ greatly after the production of mid-IR radiation and we describe each in more detail below.

The FWM apparatus illustrated in Figure 1 is based a four-beam interferometer that collects the heterodyned vibrational echo response as a function of one frequency and two time variables. The three IR pulses that focus into the sample produce the vibrational echo

response. The two time variables in between the two pairs of pulses are commonly known as the evolution time and the waiting time. The evolution time, τ, is the time delay between the first and second pulses, and the waiting time, T, is the time delay between the second and third pulses. The vibrational echo response overlaps in space and time with a fourth electric field, the local oscillator, for heterodyned detection.

A monochromator disperses the signal and local oscillator to measure the intensity of the heterodyned response as a function of the frequency axis ω_3 that is conjugate to the time delay between the third interaction pulse and the local oscillator. The monochromator scans ω_3 while a delay stage steps τ at a fixed value of T. The interference between the echo and the local oscillator produces an interferogram as a function of τ for each frequency value in ω_3. A Fourier transform with respect to the τ axis converts it to the frequency domain and provides the ω_1 frequency axis in the 2D IR spectrum.

ZnSe beam splitters divide the mid-IR radiation to create the three pulses that generate the echo response. Mechanical stages fitted with retroreflectors scan τ and T. A 3° CaF2 wedge sends a small portion of the third beam to a fourth delay stage to become the local oscillator. Square gold-coated mirrors form the three pulses into a boxcar geometry after the delay stages. A 90° off-axis parabolic mirror (100 mm focal length) focuses the three beams in the sample to a focal spot size of approximately 150 μm, and a second parabolic mirror collimates the light after the sample. An iris isolates the third order response in the $-\mathbf{k1}+\mathbf{k2}+\mathbf{k3}$ phase-matching direction after the second parabolic mirror. A 2-inch 3° CaF2 wedge combines the third-order signal and the local oscillator after the sample. A lens focuses them both through the entrance slit of a commercial monochromator. The monochromator sends its output through the exit slit to a single-channel HgCdTe (MCT) detector. The stage that controls the τ axis undersamples the interferogram with 11 fs steps from 0 to 3500 fs to collect the rephasing spectrum and from −3500 fs to 0 fs to collect the non-rephasing spectrum. The monochromator scans the ω_3 axis from 2180 cm^{-1} to 2100 cm^{-1} with 2 cm^{-1} steps. The sum of the rephasing and nonrephasing spectra produces an absorptive 2D IR spectrum.

A mechanical chopper blocks every other laser shot in one of the input beams. A gated integrator integrates and holds the detector response, and a lock-in amplifier (Stanford Research Systems) isolates the contribution to that response that depends on the beam being chopped. We set the lock-in time constant to 10 ms, so the signal is the average of ~5 laser shots since the chopped shots do not produce signal.

The pulse-shaper apparatus, modeled after the design of Shim et al,[36] is a zero-dispersion stretcher with a Ge-based acousto-optic modulator (AOM) at the Fourier plane. An arbitrary waveform generator (AWG) sends a 75 MHz acoustic wave to the Ge. The acoustic wave creates a diffraction grating in the AOM. The phase and amplitude of the acoustic wave sets the phase and amplitude of the diffracted pump beam. The AWG sends a new acoustic wave to the AOM on every laser shot, meaning that we can change the pulse shape on every laser shot.

The pulse-shaper apparatus, illustrated in Figure 2, produces a 2D IR spectrum in a pump-probe experimental geometry. The pump beam provides the first two electric-field interactions, and the probe beam is the last electric-field interaction and the local oscillator. Figure 3 shows the beam geometries at the sample in the pump-probe apparatus (A) and with a boxcar arrangement (B). An uncoated CaF2 wedge reflects a small portion of the mid-IR radiation to become the probe beam. The remaining mid-IR light is the pump beam and goes to the pulse shaper. Figure 2 shows the optical layout of the pulse-shaping apparatus, and the zero-dispersion stretcher. The pulse shaper employs frequency-domain

shaping to create two pulses in the pump beam, and scans the time delay between them, τ. The pulse shaper also controls the relative phases of the two pump pulses, which allows phase cycling. Phase cycling isolates the signal from the background, removes scattered light contributions, subtracts transient absorption signals, and shifts the signal to the rotating frame to allow a larger fully sampled step size.[1, 2, 37–39] The pulse shaper shifts the observed frequency by 1800 cm^{-1} and fully samples the observed ~355 cm^{-1} oscillation with 24 fs steps.

The time delay between the pump and probe beams is the waiting time, T. The shaped pump beam propagates to a mechanical delay stage fitted with a retroreflector to control T. A 90° off-axis parabolic mirror focuses the pump and probe beams in the sample to approximate beam diameters of 150 and 100 μm respectively. A second parabolic mirror collimates the probe beam after the sample and then sends it to the detection system.

Two different detection systems collect spectra on the pulse-shaper apparatus. Both detection systems disperse the probe beam in a spectrometer. One method scans the grating angle and collects the probe spectrum with a single-channel MCT detector similar to the four-wave mixing apparatus, except that we collect the integrated intensity of the probe beam on every laser shot rather than using the lock-in amplifier so that we can take advantage of the ability to phase cycle with the pulse shaper. The second detection system collects the entire spectrum of every laser shot with a CMOS array. Figure 4 illustrates the two different detection systems for the pulse-shaping apparatus.

The CMOS array is a Si-based visible detector, so the probe beam must be upconverted to the visible. The 50/50 beam splitter at the beginning of the apparatus dumps the excess light from our amplifier, which provides the 800 nm light for upconversion. In principle, however, other leftover beams, such as the 800 nm pump light that is dumped after pumping an optical parametric amplifier, could provide this 800 nm light for upconversion. A waveplate/polarizer combination attenuates the upconversion light. A three-optic zero-dispersion stretcher based on an 1800 g/mm grating (Richardson Gratings) and a 500 mm EFL spherical mirror with a variable-width slit (Newport SV-0.5) at the Fourier plane produces the narrow-band 800 nm beam that upconverts the IR probe beam. Both the width of the slit and its position along the Fourier plane are adjustable to control the bandwidth and center frequency of the output, respectively.

An 800 nm dichroic mirror on CaF2 that transmits IR light combines the bandwidth-narrowed 800 nm light and the IR probe beam. Lenses, placed just before the dichroic mirror in each arm, focus the narrowband 800 nm and mid-IR beams to approximate beam diameters of 30 μm and 200 μm, respectively. The beams co-propagate into a wedged 5×5×3 mm MgO:LiNbO$_3$ crystal (θ=46.5°, type I, Crylight Photonics) placed at the focus. Sum frequency generation in the crystal produces broadband visible light near 685 nm, whose spectral profile reflects that of the original IR pulse. We adjust the intensity of the narrowband 800 nm light until the sum frequency radiation is ~90% of the total bit depth of the detector. At typical IR and upconversion pulse energies, approximately 0.25 μJ and 1 μJ respectively, the sum frequency output is visible to the naked eye.

A lens focuses the upconverted visible light into a 300 mm focal length spectrometer (Princeton Instruments 2300i). A 1024-pixel single-line CMOS array (Imaging Solutions Group LW-ELIS-1394A) placed at the focal plane of the spectrometer measures the upconverted probe spectrum on every laser shot. The CMOS camera is not sold as a focal-plane array ready to be mated to a spectrometer. A custom flange connects to the mounting holes on the front of the camera body, and mates to the spectrometer. The simple mounting flange is the only alteration to the camera body required to place the array at the focal plane;

the mounting plate on the spectrometer allows adjustment along the focal axis to place the array precisely at the focal plane of the spectrometer. The camera is compatible with NI-IMAQdx drivers, so adaptation of the camera for IR spectroscopy is straightforward with LabView™ IMAQdx software. We developed all camera-control software in LabView™.

The camera connects to a computer via a FireWire™ cable. The FireWire™ cable provides power to the camera and transfers data from the onboard 14-bit A/D converter to the computer. The camera requires a differential line-rate trigger with TTL levels. A homebuilt circuit converts a normal TTL-level 1 kHz trigger that is synchronous with the laser output to a differential trigger that transmits to the camera via a custom cable provided by the manufacturer. We must also synchronize the camera triggers with the masks sent to the arbitrary waveform generator (AWG) for pulse shaping the IR, pump light. The same custom circuit gates the triggers for the camera and the AWG so that it triggers the camera only when masks are sent to the AWG. A counter on a standard multifunction DAQ card (NI PCI-6036E) controls the gate on both triggers to ensure the camera and AWG each receive the same number of triggers and remain synchronous.

The bandwidth of the 800 nm radiation limits the absolute resolution of the spectrometer. The pixel pitch of the CMOS detector is 7.8 μm, corresponding to a detector-limited resolution and bandwidth of ~0.4 cm^{-1} and ~400 cm^{-1}, respectively, when using a 1200 g/mm grating with the 300 mm spectrometer. The FWHM of the 800 nm light is ~0.2 nm, which corresponds to ~3 cm^{-1} resolution in our spectrometer. We can improve the resolution by narrowing the slit width in the 800 nm pulse shaper and can use a diffraction grating with a higher groove density to adjust the detector-limited bandwidth and resolution.

We adjust the concentration of MeSCN to find the detection threshold of the FWM apparatus. The lowest measurable concentration at which we can phase the data is ~120 mM with the current IR power (6 μJ per pulse), focusing conditions (~150 μm focal spot), and laser stability. Note that all of these conditions could be improved to decrease the threshold concentration. At the threshold concentration, the four-wave mixing apparatus cannot detect the signal at longer waiting times (T > 5 ps). We measure the waiting-time dependence of the signal in a sample with a concentration of 240 mM. Two CaF_2 windows separated by a 50 μm Teflon spacer hold the sample. FTIR spectra confirm that the absorbance of all samples is consistent. We purchase the MeSCN from Acros Organics and the DMF from Sigma-Aldrich and use all chemicals as received.

As a demonstration of the capabilities of the spectrometer, we also report a 2D IR spectrum of the protein dihydrofolate reductase (DHFR) that we cyanylated at the two native cysteines. Wild type *Escherichia coli* DHFR is expressed and purified as described elsewhere.[40] 250 μl of 2–3 mM DHFR is washed several times by centrifugal membrane filtration (MW cutoff of 10 kDa) in 100 mM KH_2PO_4 buffered to pH 7.0. Cyanylation of DHFR is carried out by the method described by Fafarman et al.[41] 2.5 molar equivalences of Ellman's Reagent[42] (5,5'-dithiobis(2-nitrobenzoic acid))(DTNB, Sigma) prepared in 100 mM KH_2PO_4 are added to DHFR, which has 2 naturally occurring cysteine residues, and incubated for 1 hour. DTNB reacts with the cysteine thiols to form disulfide linked protein-S-TNB and free TNB-, the latter of which is monitored spectrophotometrically by following the absorbance at 412 nm. After this reaction is complete, excess TNB- is washed several times from DHFR in phosphate buffer using centrifugal membrane filtration (MW cutoff of 10 kDa.) A solution of 2.4 M KCN is prepared in 200 mM KH_2PO_4, and the pH is brought to 7.2 by adding 10 μl aliquots of concentrated HCl and monitoring the pH. This solution is used to add >50 times excess KCN to the DHFR-TNB solution to displace TNB- and ultimately convert the cysteine thiol to a thiocyanate. This reaction is also monitored spectrophotometrically. Excess KCN and TNB- are washed from the cyanylated DHFR

solution using buffer and centrifugal membrane filtration. Cyanylation of DHFR is confirmed by MALDI-TOF MS and FT-IR absorbance at 2163 cm^{-1}.

Results and Discussion

The traditional FWM apparatus, with a mechanical stage and single-channel detection, collects a 2D IR spectrum in about 1 hour. The pulse-shaping apparatus with single-channel detection collects and averages 115 spectra in an hour. Continuous scanning of the τ time with the pulse shaper obviously reduces the measurement time significantly. In addition, although the FWM apparatus must scan both the rephasing and non-rephasing surfaces to sum together for the absorptive spectrum, the pulse-shaping apparatus collects the absorptive spectrum directly. Thus, for consistency we compare the S/N of a traditional FWM apparatus and a pulse-shaping one, each using a single channel detector, by collecting data for the same total laboratory measurement time. Thus, the spectra that we collect using the pulse shaper represent an average of 115 spectra, but the FWM spectra are the result of a single scan of the rephasing and non-rephasing spectra summed together to give the absorptive correlation spectrum. For the spectra collected with the upconversion detection system, we use 115 scans as we do for the single-channel detector, but this measurement is much faster than the single-channel and FWM measurements and can be completed in approximately one minute.

Figure 5 shows 2D IR spectra of 240mM MeSCN at three different waiting times (T=250 fs, 20 ps, 30 ps) collected with the FWM apparatus (top row), the pulse shaper with single-channel MCT detection (middle row), and the pulse shaper with upconversion and visible CMOS detection (bottom row). We normalize all spectra to the maximum of the 0-to-1 transition, and the contour levels vary from -1 to 1 with 21 evenly spaced intervals to allow visual comparison of the signal-to-noise levels of the spectra.

For each of the spectra, we determine the signal level from the difference between the maximum and minimum values of the peaks. To quantify the noise of the pulse-shaper spectra we calculate the RMS noise of a spectral area from $\omega_3 = 2180$ cm^{-1} to 2170 cm^{-1} and $\omega_1 = 2180$ cm^{-1} to 2100 cm^{-1}. In the data taken with the array, the noise is correlated in ω_3 because the array collects the entire ω_3 spectrum on each laser shot, and the variations in the total pulse intensity make the dominant contribution to the noise at each frequency in the probe spectrum. As a result, we calculate the noise using a region that is composed primarily of slices along the ω_1 axis. For the FWM spectra, we calculate the noise using RMS variation in the intensity in the spectral area from $\omega_1 = 2110$ cm^{-1} to 2120 cm^{-1} and $\omega_3 = 2100$ cm^{-1} to 2180 cm^{-1}. The gray boxes in the spectra in Figure 5 illustrate the areas used in the noise calculations for each of the spectra. We use a different spectral area for the noise calculation of the FWM data because a small amount of signal remains in the FWM data in the spectral range used for the pulse-shaper noise calculation. The spectrometer used to collect the FWM data had a shorter (150 mm) focal length so the resolution in ω_3 is not as high for the FWM data as for the other spectra. As a result, the signal tails to higher ω_3 frequencies in the FWM data than in the pulse-shaper spectra. In both cases, however, we have taken care to calculate the noise in areas where no signal appears.

As would be expected, the noise is essentially constant for all of the spectra taken with each data collection apparatus, regardless of the waiting time. Therefore, the reported noise is the average noise of all of the spectra for each type of data collection: FWM, pulse shaping with single-channel MCT detection, and pulse shaping with CMOS array detection. Table 1 shows the average noise for each data collection apparatus. Table 2 lists the signal and S/N of all the spectra taken. With the pulse-shaper apparatus, we collected three spectra at each waiting time for both data collection schemes. Therefore, the average noise reported for both

data collection schemes is the average of 9 spectra, and the signal reported for each waiting time is the average of 3 spectra. The signal reported for each four-wave mixing spectrum is from a single scan. The reported FWM noise is the average RMS noise calculated in the three 240 mM spectra.

The four-wave mixing apparatus, as expected, produces the greatest signal. The signal depends on the power of the three input beams and the local oscillator. The signal also greatly depends on the focal volume, as a larger energy density produces a larger signal. The focal volumes of the pulse-shaping apparatus and the four-wave mixing apparatus were matched as closely as possible as noted above. However, three beams need to overlap at the focus in the FWM apparatus, while only two beams need to overlap in the pulse shaping apparatus meaning that the interactions volumes will never be exactly the same. The initial IR power for both FWM and pulse-shaping systems is the same, but the two systems have vastly different optical setups after the production of IR radiation, so the total throughput is different. Although the throughput of the pulse shaper itself is only about 35%, the total throughput of the pulse-shaper apparatus as measured by the total power at the sample is somewhat higher than for the FWM apparatus because of the larger number of optics in the interferometer. Nevertheless, the total field strength in the FWM apparatus is greater than in the pulse shaper apparatus even though the measured power is less because the measured power is the sum of the squares of the fields rather than the square of the sum of the fields. Ultimately, at early waiting times, the signal collected by the FWM apparatus is approximately 10x greater than the signal collected with the pulse shaper using either detection system. At longer waiting times, however, the signal from the FWM apparatus appears to decrease more rapidly than with the pulse-shaping apparatus. This effect is likely the result of imperfect phase correction of the spectra and underscores one of the major challenges of the FWM apparatus. To phase correct the spectra using the projection-slice theorem the S/N ratio must be great enough to accurately compare to the pump-probe spectrum. If the S/N ratio is poor, then it will be difficult to accurately correct the phase. As a result of imperfect phase correction, the sum of the rephasing and nonrephasing spectra will lead to imperfect cancellation and summation of the dispersive and absorptive components of the line shape respectively. The imperfectly phased spectra, when summed, will then result in a smaller signal in the correlation spectrum. This phasing problem does not arise with the pulse-shaping apparatus because of the inherent phase accuracy of the shaper and of the pump-probe geometry.

The FWM spectra are single scans of the 2D IR surface, while the pulse-shaper spectra are the average of 115 scans, so the FWM spectra have significantly greater noise. The largest source of noise comes from the shot-to-shot variations of the laser intensity. Shot-to-shot fluctuations are much greater than the dark noise of either the MCT or CMOS detectors, so we assume detector noise to be negligible. Both laser systems are identical amplified systems, so the shot-to-shot fluctuations should be similar. If the noise scales ideally, and both systems produce the same noise, then the noise should scale as $\frac{1}{\sqrt{N}}$, where N is the number of shots averaged for each point. A lock-in amplifier with a 10 ms time constant collects the FWM signal; therefore, each time step is effectively the average of ~10 laser shots. The pulse shaper uses a 4-pulse phase cycle, so each time step is the average of 4 laser shots. Therefore, after averaging 115 spectra, each time point is the average of 460 laser shots. If our assumption that the shot-to-shot fluctuations of the local oscillator are the dominant noise source is correct, then the difference in the noise for the single-channel pulse-shaper spectra and the FWM spectra should be given by the square root of the ratio of the number of laser shots per point, i.e. $\mathrm{noise}_{shaper} = \mathrm{noise}_{\mathrm{FWM}} \sqrt{\frac{N_{\mathrm{FWM}}}{N_{shaper}}}$. For our

experiments, then, the noise of the shaper spectra should be $0.025 \sqrt{\frac{10}{460}} = 0.0037$, which is in perfect agreement with our measurements, supporting our assertion that shot variations of the laser are the dominant noise source. Thus, the pulse-shaper apparatus results in less noise because we average more laser shots per spectrum than in the FWM spectra. This averaging is only possible because of the inherent phase accuracy of the pulse-shaper apparatus. We would not be able to do this kind of averaging on our FWM apparatus because we would still need to be able to phase correct each individual 2D IR spectrum because the phase errors are not consistent from one measurement to the next.

The noise on the upconverted signal should, in principle, be greater than for the singlechannel data because of the additional nonlinear process, but our experiments show that the spectra taken with the CMOS array have lower noise than those taken with the single-channel detector. This result suggests that the benefits of array detection outweigh the noise of the additional nonlinear process. Specifically, the CMOS array collects 115 spectra in about a minute, while the single-channel MCT detector collects 115 spectra in about an hour. The decreased data collection time substantially reduces noise associated with long-term drift of the laser system. The array also collects the entire ω_3 spectrum of every laser shot, so there is no shot-to-shot noise across the ω_3 axis. The additional noise due to the sum frequency process must be less than the noise reduction benefits associated with more rapid data collection using the array. Of course, this benefit would also be expected when using an MCT array.

As expected, the signal for the pulse-shaping apparatus in the pump-probe geometry is much smaller than for the FWM apparatus. The spectra collected with the single-channel pulseshaper apparatus have signal amplitudes that are more than a factor of 10 smaller than in those collected with the FWM apparatus. This difference results from the fact that in the FWM apparatus, the intensities of the third interaction and the local oscillator are independently controlled. Indeed, this feature is a key advantage of the FWM method.

Interestingly, the signal in the pulse-shaping experiments with the two different detection methods is not the same. This result is somewhat surprising since the spectra with these two different detection systems were collected at the same time, switching back and forth between detection systems after making repeated measurements for each waiting time. There were no changes to the laser alignment or the energy distributions in either the pump or probe beams between these measurements. As a result, the differences in the signals between the singlechannel and CMOS array detected spectra must be the result of differences in the detection systems. Consistently in all of the spectra, the signal for the spectra collected using the CMOS array with upconversion is approximately 40% larger than in the corresponding spectra taken with the single-channel MCT detector. This result is likely due to the increased dynamic range of the CMOS array, which allows us to upconvert a larger fraction of the probe beam effectively increasing the amount of light that reaches the detector. Since the signal is the difference of phase-cycled spectra, more light reaching the detector will result in a larger absolute signal and thus a larger difference between phase-cycled shots, effectively increasing the total signal.

The current CMOS detector does come with some important limitations that should be noted as well. First, the on-board A/D convertor only has 14-bit resolution. This effectively imposes a limit on the minimum OD change that can be measured on a single scan of 0.06 mOD. Smaller differences require considerable signal averaging. Nevertheless, the signals we report are all in the range of tenths to hundredths of a mOD and we demonstrate measurements of signals as low as 0.003 mOD (*vide infra*). Clearly, a higher bit depth camera would improve our apparatus, and these are available commercially, but this

limitation is not prohibitive. A second weakness of this approach is that it does not easily lend itself to shot referencing as is often employed with two-stripe MCT array detectors. Referencing can improve the S/N ratio by as much as a factor of 10. In the upconversion apparatus, referencing would require a two-line camera, which is available, but would likely be somewhat less effective because it would be difficult to make the signal and reference upconversions identical. Finally, the current upconversion apparatus is limited to wavelengths shorter than ~5 μm (2000 cm^{-1}) because of absorption in the MgO:LiNbO$_3$ crystal. Recent reports from Marie Louise Groot's group, however, demonstrate upconversion at wavelengths out to ~10 μm (1000 cm^{-1}) using AgGaGeS$_4$.[43]

Combining the signal and noise measurements into the critical figure of merit, the S/N ratio, we find that at early waiting times the S/N for the single-channel measurement with the pulse shaper is a factor of 2 worse than in the FWM experiment, but at later waiting times, where imperfect phase correction of the data reduces the signal amplitude in the FWM experiment, the S/N ratio of these two apparatuses are nearly the same. This result is, of course, unique to the case where the signal approaches the limit of detection. For the spectra taken with the pulse shaper and the CMOS array, however, the improvement in the noise as a result of the rapid data collection and the increase in the signal compared to the single-channel MCT detector result in a S/N ratio that is a factor of 2 greater than for the single-channel detector at all waiting times and is as good or slightly better than the S/N ratio for the FWM data at all waiting times. These results show that the advantages of pulse shaping, specifically the rapid scanning of the τ time axis by changing the pulse shape on every laser shot, the ability to phase cycle the pump beams to isolate the desired third-order response, and, perhaps most importantly, the phase accuracy and stability that allow for on-the-fly averaging of the spectra, result in a measurement where the S/N ratio is as good as with a conventional FWM apparatus.

It is worth noting that incorporation of features like active phase stabilization, quasi-phase cycling, balanced detection, and rapid scanning in the FWM apparatus would certainly lead to a superior result compared to the pulse-shaping apparatus we report, but these improvements would also substantially increase the complexity of the experiment. This increase in complexity has been a significant barrier to more widespread adoption of these improvements. In contrast, the pulse-shaper apparatus is, comparatively, much easier to align and work with on a day-to-day basis and there is even a commercial version available from Phasetech Spectroscopy that can easily be implemented in an existing IR pump-probe apparatus.

The biggest advantage of the pulse shaper is the ability to directly acquire correctly phased data. The collection of perfectly phased data offers several important benefits. First, data analysis is greatly simplified. The experimenter does not need to collect a pump-probe spectrum for every 2D spectrum to properly phase the data; therefore, data collection is expedited. Second, the experimenter can average the spectra during data collection, so the signal on a single scan does not need to be above the noise background. Extended averaging allows the observation of signals that cannot be detected with the traditional FWM apparatus. The lowest easily detectable concentration of MeSCN in DMF taken with our traditional FWM apparatus with the current IR power (6 μJ per pulse), focusing conditions (~150 μm focal spot), and laser stability is 120 mM. Figure 6 shows the 2D IR spectra of 120 mM MeSCN taken with the three different data collection methods. Imperfect phasing of the rephasing and non-rephasing spectra from the FWM experiment results in an extra peak in the correlation spectrum. In fact, the non-rephasing signal is almost unidentifiable at this concentration.

For comparison and as a demonstration of the potential to detect the signal from weak chromophores at low concentrations, Figure 7 shows the 2D IR spectrum of cyanylated dihydrofolate reductase (DHFR) in water, taken with the pulse shaper and CMOS array detector averaging 150,000 scans for T = 1000 fs. DHFR is a small protein with two cysteine groups. Cyanylated cysteines have an extinction coefficient of 130 $M^{-1}cm^{-1}$.[41] Thus, this chromophore is even weaker than MeSCN. There are two cyanylated cysteines for each DHFR molecule and the total concentration of DFHR in the sample is 2.32 mM yielding a effective concentration of chromophores of 4.64 mM. The two cyano groups are indistinguishable and thus contribute to the spectrum additively. The signal is very weak and the measurement is extremely challenging, so we do increase the total IR power to 15 μJ per pulse and improve the focusing condition so that the IR beam diameter at the sample is approximately 50 μm for both pump and probe beams. In addition, the signal is more difficult to resolve in water because water is not background-free at 2160 cm^{-1} and absorbs some of the emitted signal. Furthermore, the water itself generates a background signal that becomes significant at these low signal levels and must be subtracted off. There are several previous studies of weak chromophores at low concentrations using FWM,[44–46] but there have been no previous reports of such a weak signal using a pulse shaper leading to uncertainty about whether such experiments are possible with this apparatus. This measurement demonstrates that signal averaging, made possible through the inherent phase accuracy and stability of the pulse shaper, enables the observation of very weak signals and shows that such systems are still accessible with an apparatus using a pulse shaper in the pump-probe geometry in spite of the decreased signal level inherent with this beam geometry. To our knowledge this spectrum is the first example of a 2D IR measurement of a cyanylated cysteine in a protein, and this result demonstrates the measurement of a signal that is as small as any reported in the literature to date.

Conclusions

This manuscript compares the S/N measured with a traditional FWM apparatus to the S/N measured with a pulse-shaping apparatus to assess the ability of the pulse-shaping apparatus to access weak chromophores at low concentrations. We choose the sample concentration for the comparison based on the smallest easily phase corrected signal using the traditional FWM apparatus. Under our experimental conditions, the pulse-shaping apparatus with the CMOS array detector and upconversion of the IR light into the visible results in spectra with a similar S/N ratio as with the conventional FWM apparatus. The pulse shaping apparatus can detect much smaller signals because of the potential for signal averaging. A traditional four-wave mixing apparatus cannot average signals that are not detectable in a single scan, because each spectrum requires correction of the frequency-dependent phase. A fully optimized FWM spectrometer should produce greater S/N than what is presented here, but we compare the pulse shaper to a conventional FWM apparatus, without active phase stabilization, quasi-phase cycling, balanced detection, and rapid scanning, which is similar to what is in widespread use. Furthermore, we demonstrate that the benefits of array detection significantly outweigh the noise due to upconversion and that the increased dynamic range of the CMOS detector compared to MCT actually increases the measured signal with this detector. We demonstrate the potential of this apparatus to access weak chromophores in dilute solutions by measuring the 2D IR spectrum of the protein DHFR with two cyanylated cysteines.

Acknowledgments

References

1. Hamm, P.; Zanni, MT. Concepts and Methods of 2D Infrared Spectroscopy. New York, NY: Cambridge University Press; 2011.

2. Shim SH, Strasfeld DB, Ling YL, Zanni MT. Automated 2D IR Spectroscopy Using a Mid-Ir Pulse Shaper and Application of This Technology to the Human Islet Amyloid Polypeptide. Proc. Natl. Acad. Sci. U.S.A. 2007; 104:14197–14202. [PubMed: 17502604]

3. Strasfeld DB, Ling YL, Shim SH, Zanni MT. Tracking Fiber Formation in Human Islet Amyloid Polypeptide with Automated 2D-IR Spectroscopy. J. Am. Chem. Soc. 2008; 130 6698-+

4. Grumstrup EM, Shim SH, Montgomery MA, Damrauer NH, Zanni MT. Facile Collection of Two-Dimensional Electronic Spectra Using Femtosecond Pulse-Shaping Technology. Opt. Express. 2007; 15:16681–16689. [PubMed: 19550954]

5. Xiong W, Zanni MT. Signal Enhancement and Background Cancellation in Collinear Two-Dimensional Spectroscopies. Opt. Lett. 2008; 33:1371–1373. [PubMed: 18552963]

6. Shim SH, Gupta R, Ling YL, Strasfeld DB, Raleigh DP, Zanni MT. Two-Dimensional IR Spectroscopy and Isotope Labeling Defines the Pathway of Amyloid Formation with Residue-Specific Resolution. Proc. Natl. Acad. Sci. U.S.A. 2009; 106:6614–6619. [PubMed: 19346479]

7. Strasfeld DB, Ling YL, Gupta R, Raleigh DP, Zanni MT. Strategies for Extracting Structural Information from 2D IR Spectroscopy of Amyloid: Application to Islet Amyloid Polypeptide. J. Phys. Chem. B. 2009; 113:15679–15691. [PubMed: 19883093]

8. Woys AM, Lin YS, Reddy AS, Xiong W, de Pablo JJ, Skinner JL, Zanni MT. 2D IR Line Shapes Probe Ovispirin Peptide Conformation and Depth in Lipid Bilayers. J. Am. Chem. Soc. 2010; 132:2832–2838. [PubMed: 20136132]

9. Middleton CT, Strasfeld DB, Zanni MT. Polarization Shaping in the Mid-IR and Polarization-Based Balanced Heterodyne Detection with Application to 2D IR Spectroscopy. Opt. Express. 2009; 17:14526–14533. [PubMed: 19687931]

10. Strasfeld DB, Shim S-H, Zanni MT. Rice SA. New Advances in Mid-IR Pulse Shaping and Its Application to 2D IR Spectroscopy and Ground-State Coherent Control. Advances in Chemical Physics. 2009; Vol 141:1–28. Vol. 141.

11. Shim S-H, Zanni MT. How to Turn Your Pump-Probe Instrument into a Multidimensional Spectrometer: 2D IR and Vis Spectroscopies Via Pulse Shaping. Phys. Chem. Chem. Phys. 2009; 11:748–761. [PubMed: 19290321]

12. Tekavec PA, Lewis KLM, Fuller FD, Myers JA, Ogilvie JP. Toward Broad Bandwidth 2-D Electronic Spectroscopy: Correction of Chirp from a Continuum Probe. IEEE Journal of Selected Topics in Quantum Electronics. 2012; 18:210–217.

13. Turner DB, Stone KW, Gundogdu K, Nelson KA. Invited Article: The Coherent Optical Laser Beam Recombination Technique (Colbert) Spectrometer: Coherent Multidimensional Spectroscopy Made Easier. Review of Scientific Instruments. 2011:82.

14. Tian PF, Keusters D, Suzaki Y, Warren WS. Femtosecond Phase-Coherent Two-Dimensional Spectroscopy. Science. 2003; 300:1553–1555. [PubMed: 12791987]

15. Keusters D, Tan HS, Warren WS. Role of Pulse Phase and Direction in Two-Dimensional Optical Spectroscopy. J. Phys. Chem. A. 1999; 103:10369–10380.

16. Myers JA, Lewis KLM, Tekavec PF, Ogilvie JP. Two-Color Two-Dimensional Fourier Transform Electronic Spectroscopy with a Pulse-Shaper. Opt. Express. 2008; 16:17420–17428. [PubMed: 18958024]

17. Dutta S, Rock W, Cook RJ, Kohen A, Cheatum CM. Two-Dimensional Infrared Spectroscopy of Azido-Nicotinamide Adenine Dinucleotide in Water. J. Chem. Phys. 2011; 135:055106–6. [PubMed: 21823737]

18. Kumar SKK, Tamimi A, Fayer MD. Comparisons of 2D IR Measured Spectral Diffusion in Rotating Frames Using Pulse Shaping and in the Stationary Frame Using the Standard Method. J. Chem. Phys. 2012; 137:184201. [PubMed: 23163363]

19. Hybl JD, Christophe Y, Jonas DM. Peak Shapes in Femtosecond 2D Correlation Spectroscopy. Chem. Phys. 2001; 266:295–309.

20. Yetzbacher MK, Belabas N, Kitney KA, Jonas DM. Propagation, Beam Geometry, and Detection Distortions of Peak Shapes in Two-Dimensional Fourier Transform Spectra. J. Chem. Phys. 2007:126.

21. Cho B, Yetzbacher MK, Kitney KA, Smith ER, Jonas DM. Propagation and Beam Geometry Effects on Two-Dimensional Fourier Transform Spectra of Multilevel Systems. J. Phys. Chem. A. 2009; 113:13287–13299. [PubMed: 19780599]

22. DeFlores LP, Nicodemus RA, Tokmakoff A. Two Dimensonal Fourier Transform Spectroscopy in the Pump-Probe Geometry. Opt. Lett. 2007; 32:2966–2968. [PubMed: 17938668]

23. Fulmer EC, Mukherjee P, Krummel AT, Zanni MT. A Pulse Sequence for Directly Measuring the Anharmonicities of Coupled Vibrations: Two-Quantum Two-Dimensional Infrared Spectroscopy. J. Chem. Phys. 2004; 120:8067–8078. [PubMed: 15267726]

24. Schutz CN, Warshel A. Analyzing Free Energy Relationships for Proton Translocations in Enzymes: Carbonic Anhydrase Revisited. J. Phys. Chem. B. 2004; 108:2066–2075.

25. Roberts ST, Loparo JJ, Ramasesha K, Tokmakoff A. A Fast-Scanning Fourier Transform 2D IR Interferometer. Optics Communications. 2011; 284:1062–1066.

26. Bloem R, Garrett-Roe S, Strzalka H, Hamm P, Donaldson P. Enhancing Signal Detection and Completely Eliminating Scattering Using Quasi-Phase-Cycling in 2D IR Experiments. Opt. Express. 2010; 18:27067–27078. [PubMed: 21196983]

27. Helbing J, Hamm P. Compact Implementation of Fourier Transform Two-Dimensional IR Spectroscopy without Phase Ambiguity. J. Opt. Soc. Am. B. 2011; 28:171–178.

28. Volkov V, Schanz R, Hamm P. Active Phase Stabilization in Fourier-Transform Two-Dimensional Infrared Spectroscopy. Opt. Lett. 2005; 30:2010–2012. [PubMed: 16092249]

29. Backus EHG, Garrett-Roe S, Hamm P. Phasing Problem of Heterodyne-Detected Two-Dimensional Infrared Spectroscopy. Opt. Lett. 2008; 33:2665–2667. [PubMed: 19015702]

30. Heilweil EJ. Ultrashort-Pulse Multichannel Infrared-Spectroscopy Using Broad-Band Frequency-Conversion in LiIO3. Opt. Lett. 1989; 14:551–553. [PubMed: 19752893]

31. Moore JN, Hansen PA, Hochstrasser RM. A New Method for Picosecond Time-Resolved Infrared-Spectroscopy - Applications to CO Photodissociation from Iron Porphyrins. Chem. Phys. Lett. 1987; 138:110–114.

32. Dougherty TP, Heilweil EJ. Dual-Beam Subpicosecond Broad-Band Infrared Spectrometer. Opt. Lett. 1994; 19:129–131. [PubMed: 19829567]

33. Kubarych KJ, Joffre M, Moore A, Belabas N, Jonas DM. Mid-Infrared Electric Field Characterization Using a Visible Charge-Coupled-Device-Based Spectrometer. Opt. Lett. 2005; 30:1228–1230. [PubMed: 15945144]

34. Nee MJ, McCanne R, Kubarych KJ, Joffre M. Two-Dimensional Infrared Spectroscopy Detected by Chirped Pulse Upconversion. Opt. Lett. 2007; 32:713–715. [PubMed: 17308611]

35. DeCamp ME, Tokmakoff A. Upconversion Multichannel Infrared Spectrometer. Opt. Lett. 2005; 30:1818–1820. [PubMed: 16092356]

36. Shim SH, Strasfeld DB, Zanni MT. Generation and Characterization of Phase and Amplitude Shaped Femtosecond Mid-IR Pulses. Opt. Express. 2006; 14:13120–13130. [PubMed: 19532209]

37. Strasfeld DB, Shim SH, Zanni MT. Controlling Vibrational Excitation with Shaped Mid-Ir Pulses. Phys. Rev. Lett. 2007:99.

38. Yamashita T, Voth GA. Insights into the Mechanism of Proton Transport in Cytochrome C Oxidase. J. Am. Chem. Soc. 2012; 134:1147–1152. [PubMed: 22191804]

39. Shim, SH. 2D IR Spectroscopy: Automation with Pulse Shaping and Application to Amyloid Folding. Madison: University of Wisconsin; 2008. Ph.D. Thesis

40. Adams JA, Fierke CA, Benkovic SJ. The Function of Amino-Acid-Residues Contacting the Nicotinamide Ring of Nadph in Dihydrofolate-Reductase from Escherichia-Coli. Biochemistry. 1991; 30:11046–11054. [PubMed: 1834173]

41. Fafarman AT, Webb LJ, Chuang JI, Boxer SG. Site-Specific Conversion of Cysteine Thiols into Thiocyanate Creates an IR Probe for Electric Fields in Proteins. J. Am. Chem. Soc. 2006; 128:13356–13357. [PubMed: 17031938]

42. Ellman GL. Tissue Sulfhydryl Groups. Archives of Biochemistry and Biophysics. 1959; 82:70–77. [PubMed: 13650640]

43. Zhu J, Mathes T, Stahl AD, Kennis JTM, Groot ML. Ultrafast Mid-Infrared Spectroscopy by Chirped Pulse Upconversion in 1800-1000cm(−1) Region. Opt. Express. 2012; 20:10562–10571. [PubMed: 22565682]

44. Kuroda DG, Bauman JD, Challa JR, Patel D, Troxler T, Das K, Arnold E, Hochstrasser RM. Snapshot of the Equilibrium Dynamics of a Drug Bound to Hiv-1 Reverse Transcriptase. Nature Chemistry. 2013; 5:174–181.

45. Bloem R, Koziol K, Waldauer SA, Buchli B, Walser R, Samatanga B, Jelesarov I, Hamm P. Ligand Binding Studied by 2D IR Spectroscopy Using the Azidohomoalanine Label. J. Phys. Chem. B. 2012; 116:13705–13712. [PubMed: 23116486]

46. Kozinski M, Garrett-Roe S, Hamm P. 2D-IR Spectroscopy of the Sulfhydryl Band of Cysteines in the Hydrophobic Core of Proteins. J. Phys. Chem. B. 2008; 112:7645–7650. [PubMed: 18512974]
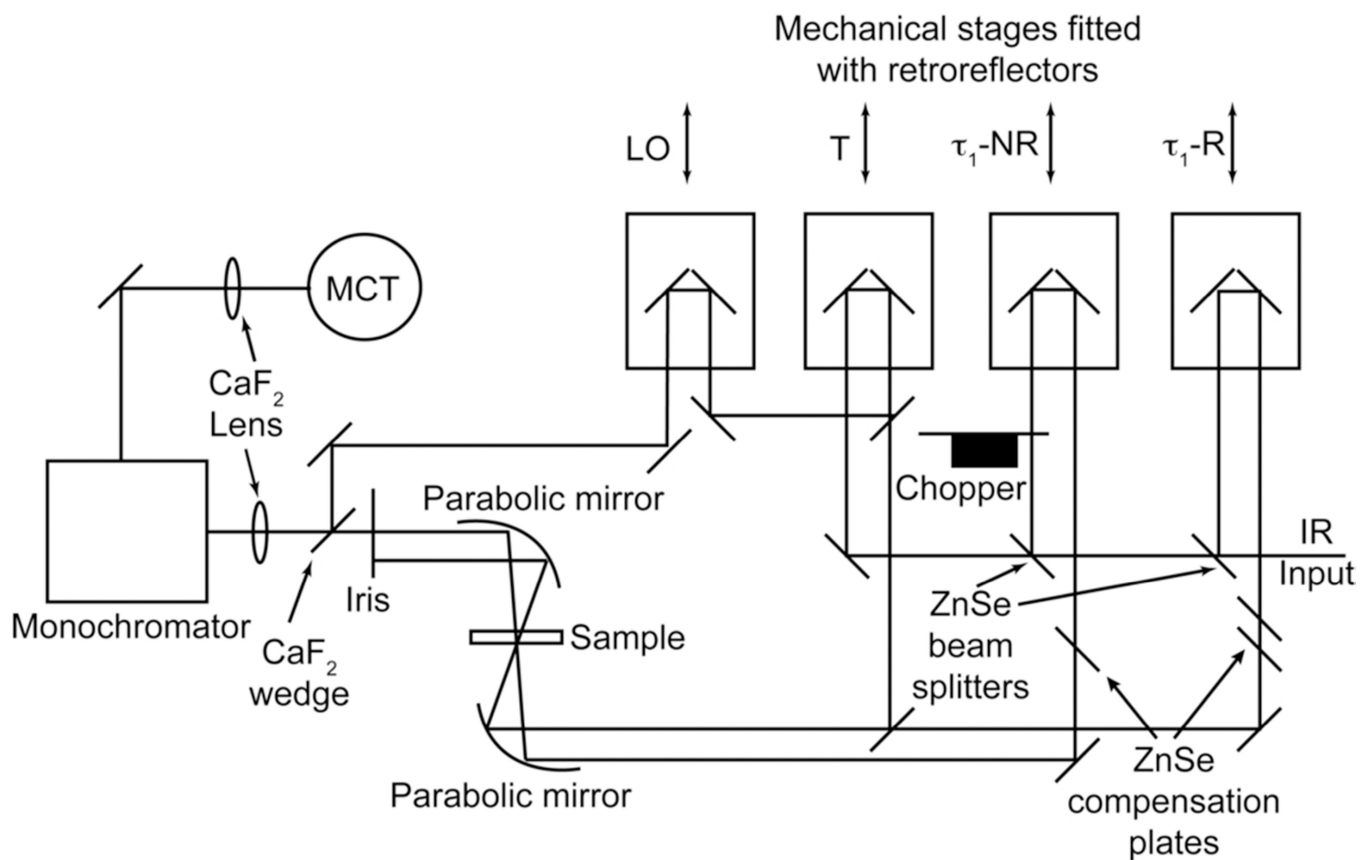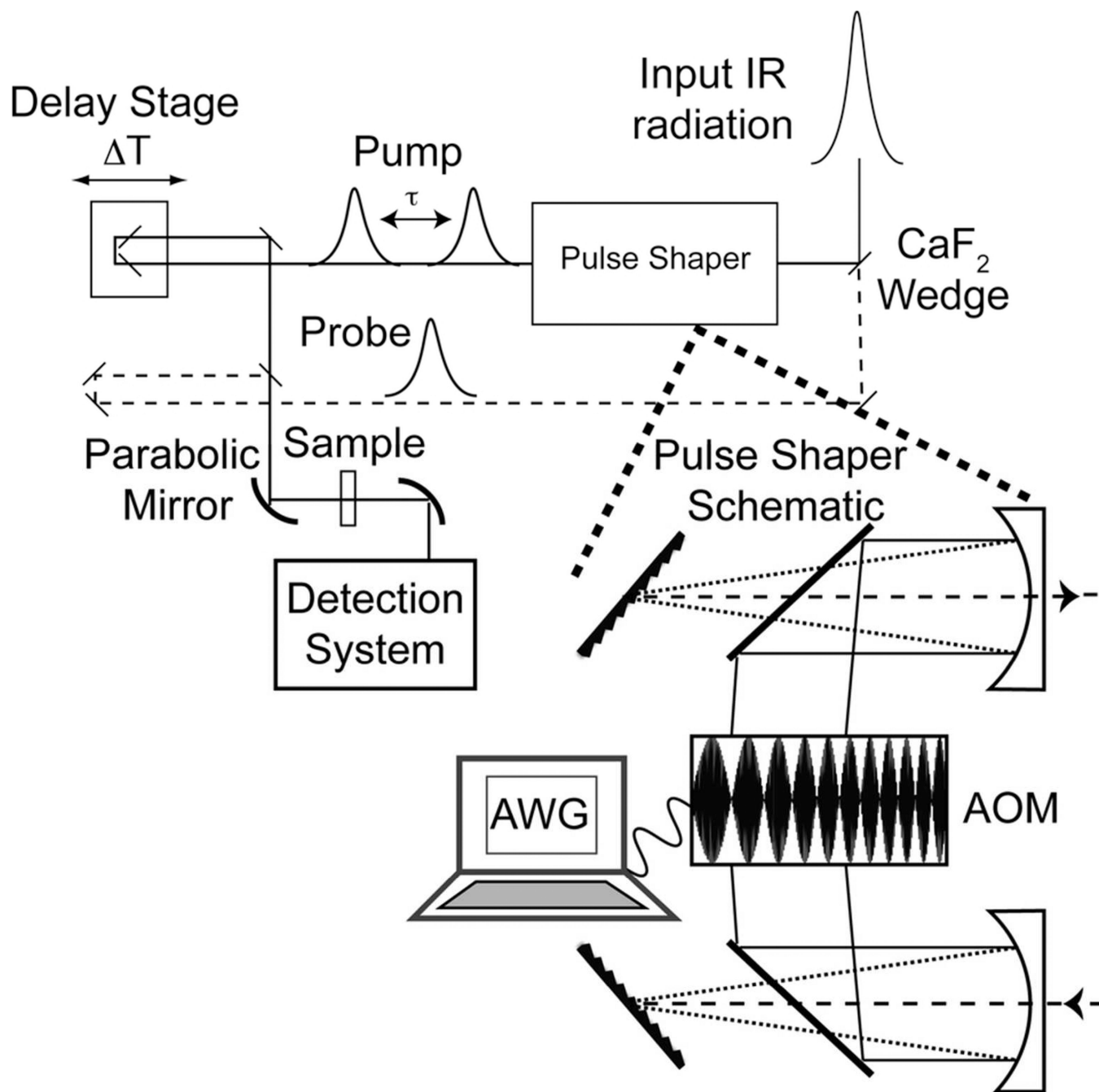
Figure 1.
Optical layout of the FWM apparatus

Figure 2.
Optical layout of the pulse-shaper apparatus: the design is identical to a pump-probe spectrometer, except that an infrared pulse shaper is placed in the pump beam. The inset shows the optical layout of the pulse shaper.
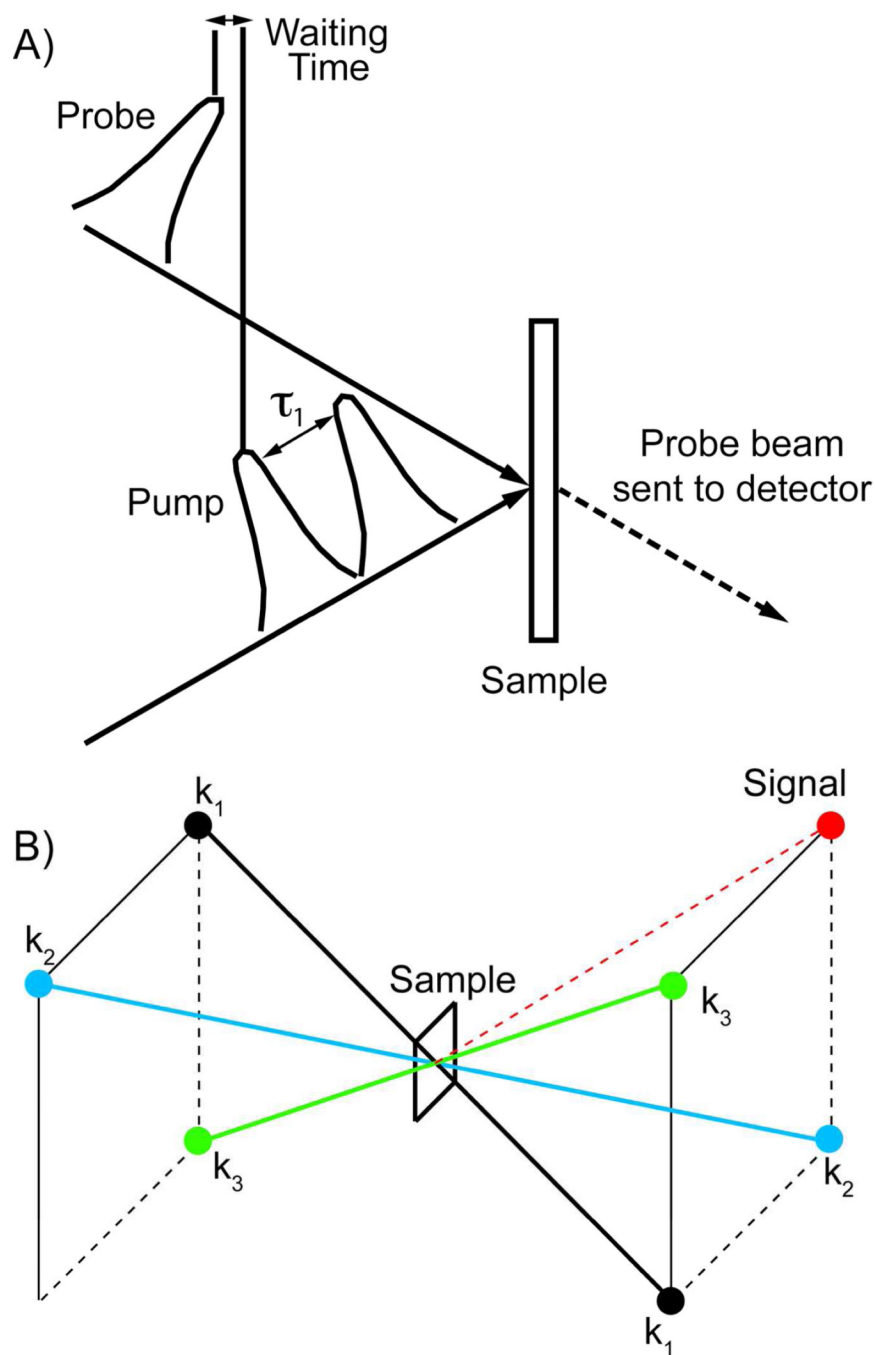
Figure 3.
Illustration of the pump-probe beam geometry (A), and the boxcar beam geometry (B) as the beams focus into the sample. The probe beam acts as the third electric field interaction and the local oscillator in the pump-probe geometry. The local oscillator is overlapped with the emitted signal after the sample in the boxcar geometry so that the intensities of the third interaction pulse and the local oscillator are independently controlled.
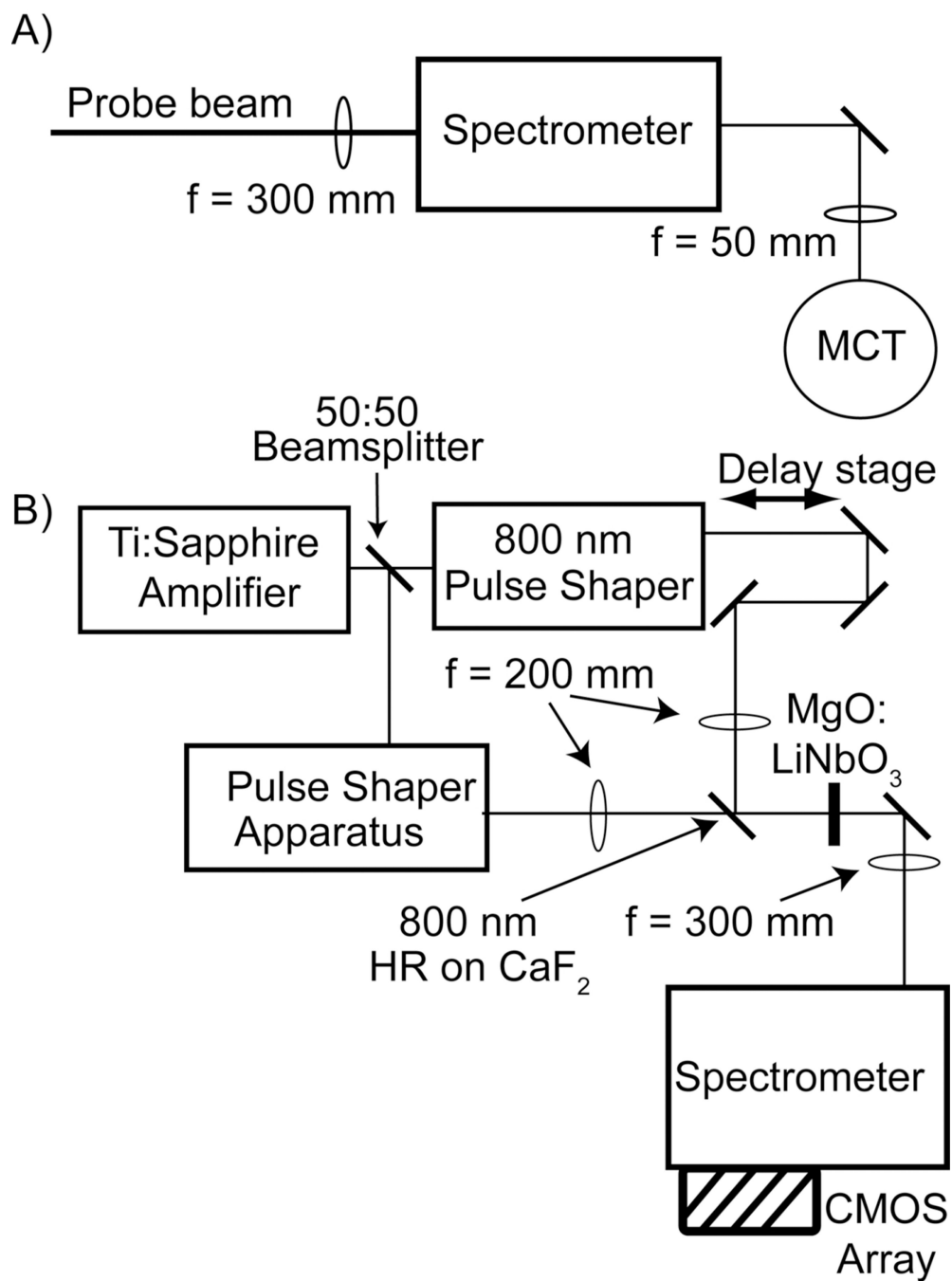
Figure 4.
Optical layout of the two detection schemes used in the pulse-shaping apparatus: (A) Single channel MCT detection scheme (B) Visible detection scheme utilizing upconversion and a CMOS array
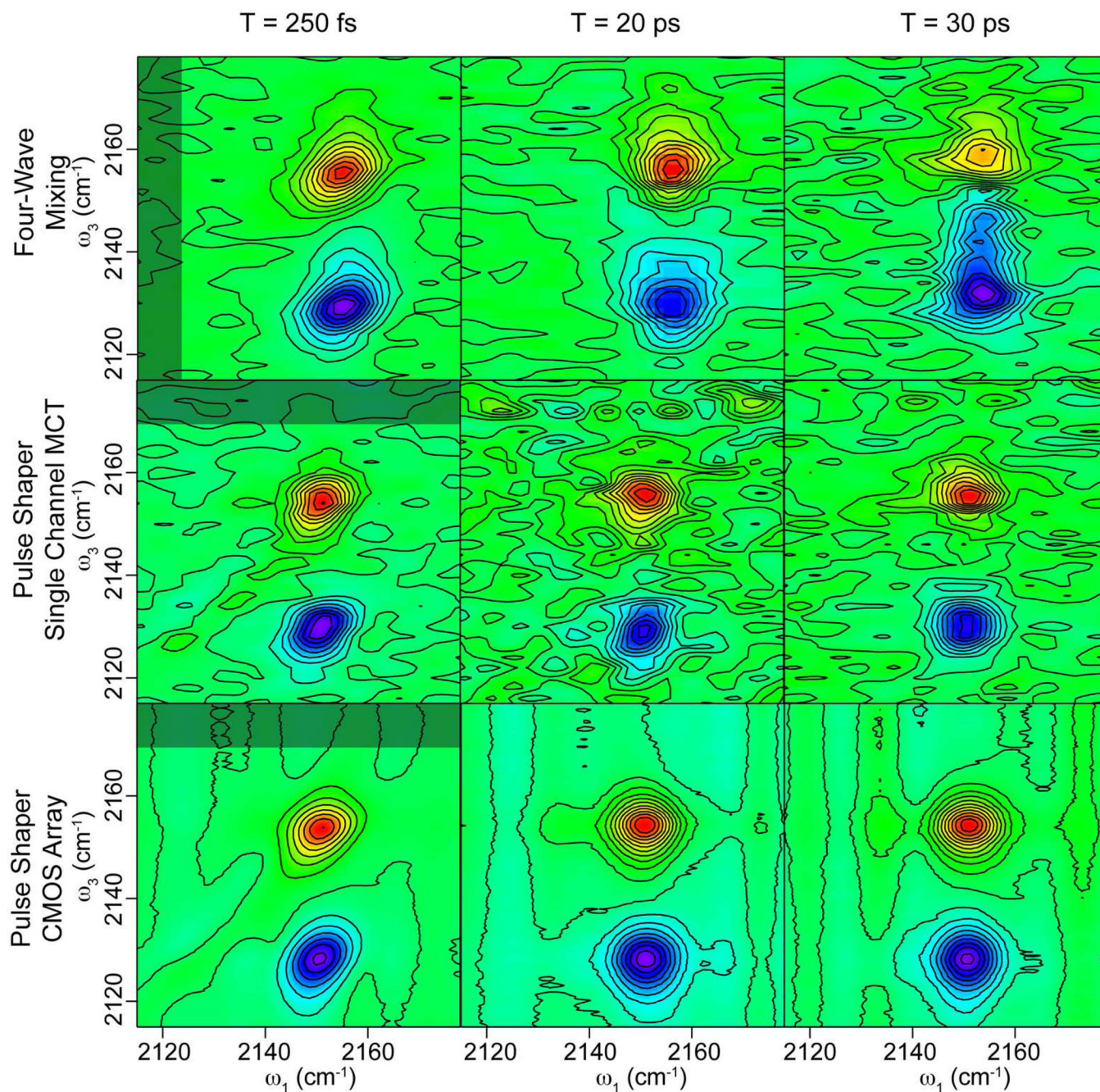
Figure 5.
The rows are spectra collected with the three apparatuses: FWM with single-channel MCT detection, pulse shaping with single-channel MCT detection, and pulse shaping with upconversion and CMOS array detection. All spectra are of 240 mM MeSCN in DMF. The columns are three different waiting times, T=250fs, 20ps, 30ps. The gray boxes on the 240 mM spectra highlight the areas used in the RMS noise calculations.
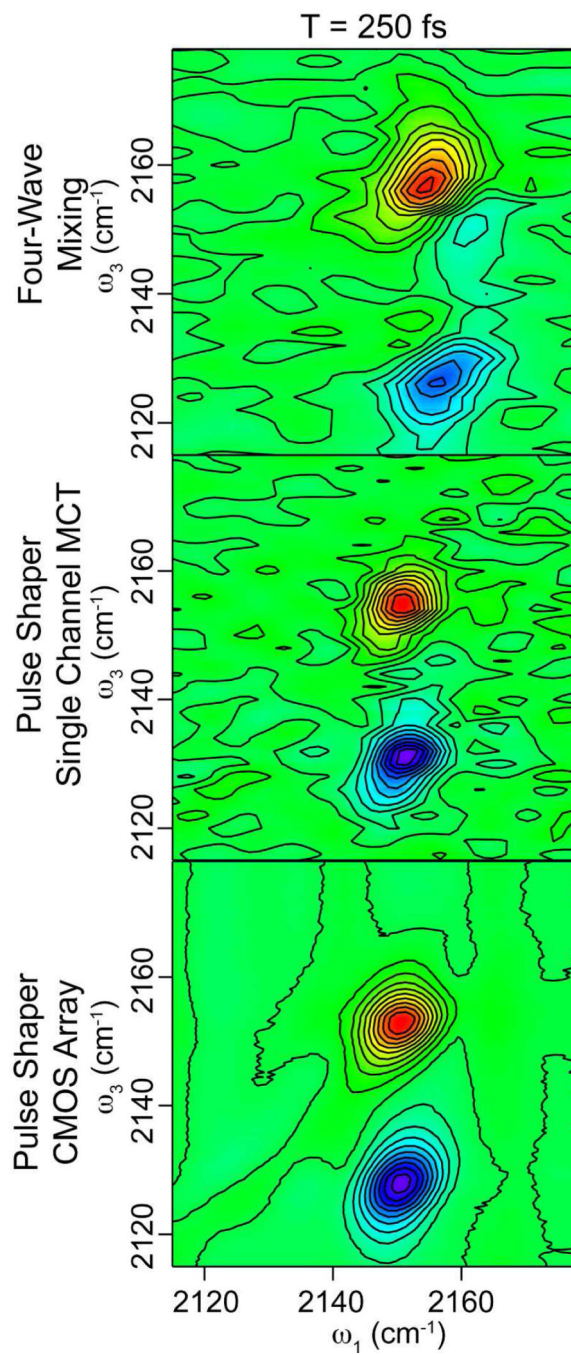
Figure 6.
2D IR spectra of 120 mM MeSCN collected with the three different data collection apparatuses. All spectra were collected under the same conditions that the 240 mM spectra were collected.
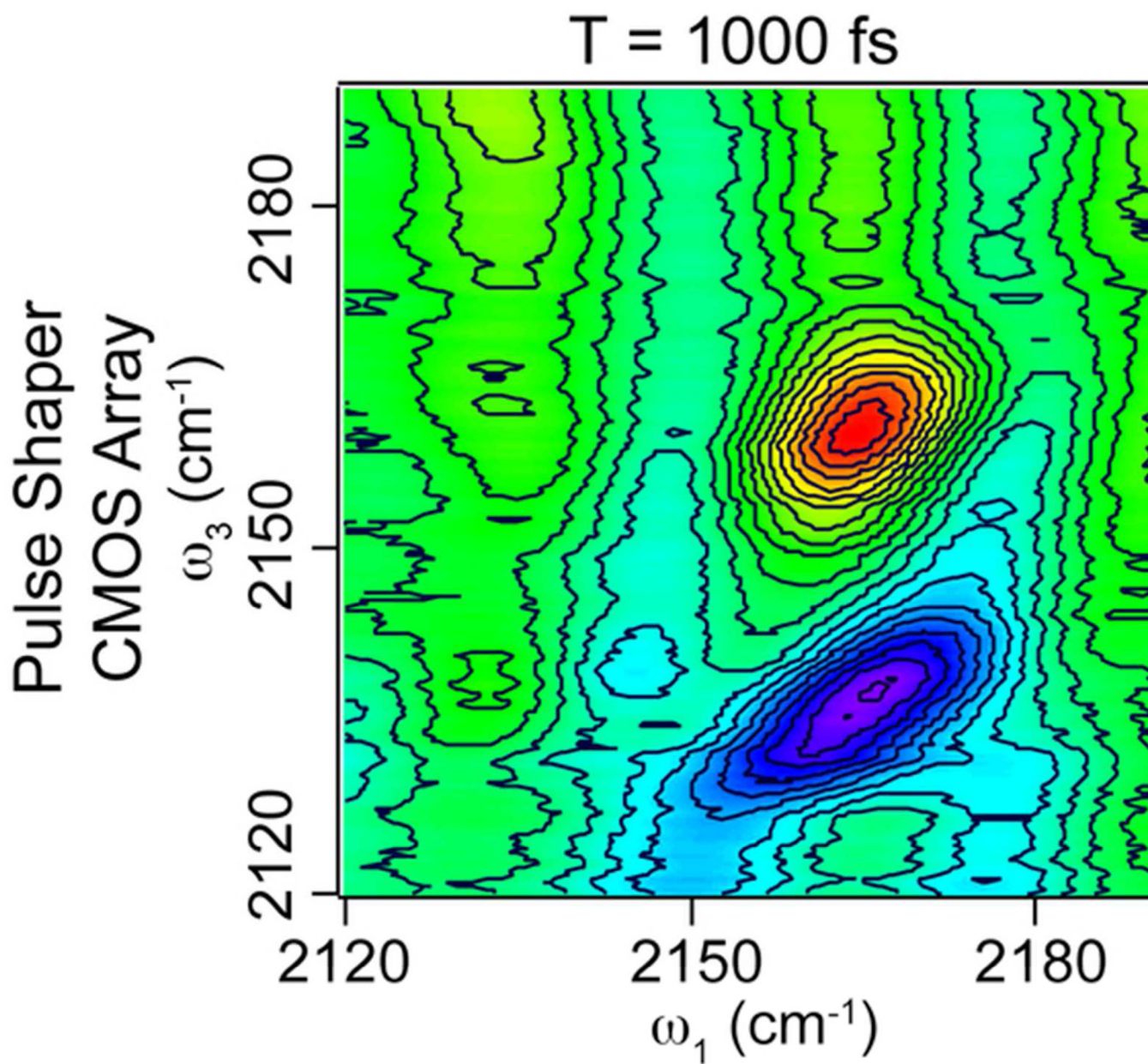
Figure 7.
The 2D IR spectrum of 2.3 mM cyanylated DHFR in water at T = 1000 fs. Each DHFR protein has two cyanylated cysteines with molar extinction coefficients of 130 $M^{-1}cm^{-1}$. The spectrum is the average of 150,000 scans of the pulse-shaping apparatus with CMOS array detection.

Table 1

The RMS noise calculated as the average noise from all spectra of each measurement type regardless of T delay.

Measurement Type	Average Noise
Four-Wave Mixing	0.025 ± 0.003
Single Channel (Pulse Shaper)	0.0037 ± 0.0005
Array (Pulse Shaper)	0.0024 ± 0.0005

Table 2

The signal and S/N measured with the three data collection methods at each T delay.

T (ps)	FWM Signal	SC Signal	Array Signal	FWM S/N	SC S/N	Array S/N
240 mM MeSCN in DMF						
0.250	2.61	0.202 ± 0.029	0.287 ± 0.002	91	56 ± 7	105 ± 13
20	0.801	0.078 ± 0.014	0.112 ± 0.001	36	22 ± 6	55 ± 8
30	0.679	0.074 ± 0.011	0.114 ± 0.002	27	23 ± 3	51 ± 13
120 mM MeSCN in DMF						
0.250	0.967	0.132 ± 0.005	0.137 ± 0.002	53	36 ± 2	88 ± 16